ARTICLE

Axial and helical thermally activated delayed fluorescence bicarbazole emitters: Opposite modulation of circularly polarized luminescence through intramolecular charge-transfer dynamics

Received 00th January 20xx,
Accepted 00th January 20xx

DOI: 10.1039/x0xx00000x

Patthira Sumsalee,[a] Laura Abella,[b] Thierry Roisnel,[a] Sabrina Lebrequier,[c] Grégory Pieters,[c] Jochen Autschbach[b,*], Jeanne Crassous[a] and Ludovic Favereau[a,*]

The rationalization of the molecular parameters that influence the intensity and sign of circularly polarized luminescence (CPL) for chiral emitters is a challenging task and remains of high interest for future chiral optoelectronic applications. In this report, we explore the design of novel chiral donor-acceptor structures based on C_2-symmetric bicarbazole systems and compare the influence of the type of chirality, namely axial *versus* helical, and the electron withdrawing strength of the acceptor units on the resulting photophysical and CPL properties. By using carbonyl-based acceptors with both axial and helical electron donors, CP-Thermally Activated Delayed Fluoresence (TADF) can be obtained, whose efficiency depends on the dihedral angle between the carbazole moieties, related to the axial and helical chirality of the compounds. The latter also impacts the intensity of the CPL, which shows an opposite trend in function of the polarity of the solvent, with notably a strong increase of the luminescence dissymmetry factor, g_{lum}, for the helical donor-acceptor compounds related to a subtle reoarganization of the intramolecular charge-transfer process.

Introduction

Designing molecular chiral materials able to emit circularly polarized luminescence (CPL) has recently attracted a strong interest owing to the potential of CP light in a diverse range of applications going from chiroptoelectronics (organic light-emitting diodes (OLEDs), optical information processing, etc.) to bio-imaging and chiral sensing.[1] In this domain, chiral lanthanide and chromium (III) complexes exhibit high intensity of CPL, with luminescence dissymmetry factors (g_{lum} = $2(I_L–I_R)/(I_L+I_R)$) up to 1.4 and 0.3, respectively, owing a combination of allowed magnetic and forbidden electric.[2] Despite their much lower CPL response (g_{lum} ~10^{-3}), chiral organic molecules are also actively investigated as potential CPL emitters owing to their readily tuneable optoelectronic properties and often higher photoluminescence quantum yield (PLQY). The latter factor, combined to the high molar extinction coefficient of their electric dipole allowed transitions, provide to organic chiral dyes potentially high level of CPL brightness,[3] which make them valuable candidates for CPL applications.[4] Moreover, organic molecules can reach very intense CPL once self-organized in condensed phases or judiciously blended in polymeric materials.[5] Currently, chemists are trying to fully rationalize the structural and electronic factors that govern the intensity and sign of CPL in chiral molecules in order to establish molecular guidelines to design emitters with higher g_{lum} values.[6] Along this objective, merging CPL with other properties such as thermally activated delayed fluorescence (TADF),[7] or CPL sign switch under external stimuli,[8] have also raised significant attention for the development of efficient CP-OLEDs and innovative chiroptoelectronic devices.

In this regard, we and others recently investigated the chiroptical properties of C_2-symmetric bicarbazole systems (Compounds A-D, Figure 1), which have displayed CPL values of up to 1.3 x 10^{-2} at the molecular level, [6e,9] highlighting the potential of these chiral building blocks as efficient CPL emitters. Moreover, we have also shown that axial bicarbazole systems substituted by benzonitrile derivatives (Compound B, Figure 1), can lead to a CPL sign inversion upon polarity increase.[10] Being still rare in the literature,[8c,d,f,g] such type of CPL switch is fundamentally interesting to completely understand the CPL phenomenon, and is of potential interest for future CPL-based optoelectronic applications, as well as bio-imaging and chiral sensing where interactions between the chiral dye and its surroundings play a crucial role.

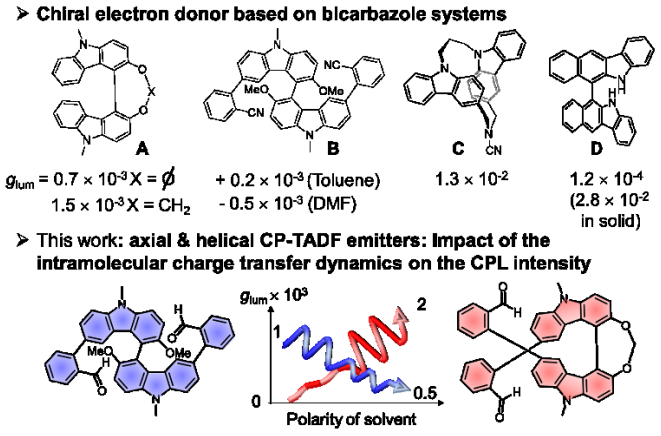

Figure 1. Top: Examples of chiral bicarbazole systems with their corresponding g_{lum} (see Ref. 6e and 9). Bottom: chemical structures of the CP-

[a] Univ Rennes, CNRS, ISCR-UMR 6226, F-35000 Rennes, France. E-mail: ludovic.favereau@univ-rennes1.fr.
[b] Department of Chemistry, University at Buffalo, State University of New York, Buffalo, NY 14260, USA. E-mail: jochena@buffalo.edu.
[c] Université Paris-Saclay, CEA, INRAE, Département Médicaments et Technologies pour la Santé (DMTS), SCBM, 91191 Gif-sur-Yvette, France.

† Footnotes relating to the title and/or authors should appear here.
Electronic Supplementary Information (ESI) available: [details of any supplementary information available should be included here]. See DOI: 10.1039/x0xx00000x

TADF emitters reported in this study with the schematic opposite evolution of their CPL intensity (blue and red for axial and helical donor-acceptor, respectively) as a function of the polarity of the solvent.

Following these promising results, we further envision to pursue the molecular engineering of this kind of electron donor unit to design innovative chiral push-pull materials. It seems notably interesting to explore these bicarbazole systems as potential chiral electron donors for the development of inherently CP-TADF chromophore,[7c,g,i,j,11] given the well-established ability of the carbazole unit to promote TADF property once functionalized with electron acceptor fragments in achiral emitters.[12] While the design of CP-TADF emitters has been applied with axial, planar and point chirality elements, combining helical chirality and TADF property remains unknown,[13] despite the rather high CPL intensity obtained for helicene-based and its derivatives chiral emitters.[14]

Here we report the synthesis, photophysical and chiroptical properties of a new family of axial and helical donor-acceptor systems based on bicarbazole electron-donor unit. When substituted with carbonyl electron acceptor groups, axially and helically chiral emitters display CP-TADF property with g_{lum} values up to 2×10^{-3}. Interestingly, playing with the torsion angle between the carbazole π-systems, and thus their resulting electronic interaction, affords important intensity differences for both TADF and CPL properties. Finally, while axial derivatives show a decrease of CPL intensity with the increase of solvent polarity, helical derivatives display a significant enhancement of g_{lum}, arising from a chiral excitonic coupling mechanism induced in both ground- and excited-states by the modulation of the intramolecular charge transfer dynamics.

Results and discussion

Synthesis and structural characterization

As mentioned above, axially chiral bicarbazole substituted with benzonitrile electron acceptor groups affords an interesting CPL sign inversion upon polarity increase, from $+2 \times 10^{-4}$ to -5×10^{-4} when going from toluene to dimethylformamide solvents. This effect has been rationalized in terms of the presence of different luminescent conformers in solution, related to the orientation of the cyano group towards the carbazole units (Figure 1). Following these findings, we envisioned to take advantage of this effect to afford innovative CP-TADF with potentially through-space charge-transfer transition, which appears a promising strategy to reach both intense TADF and CPL properties.[7g-i] To reach such objective, we notably investigated several key structural and electronic aspects on the photophysical and chiroptical properties of the obtained chiral emitters such as the impact of the torsion angle between the two carbazole systems, the type of grafted electron withdrawing groups as well as their substituted position relatively to the nitrogen atoms of the carbazole donor. In this regard, -cyano and formyl functional groups have been selected as electron withdrawing units given the use of the former for designing achiral TADF materials,[12a,b,15] and their low steric hindrance, which may favour electronic interaction with the opposite carbazole unit and result in through-space charge-transfer interaction. Moreover, carbonyl groups have been known to exhibit magnetic dipole allowed transitions,[16] which may help to reach significant intensity of CPL.

The chemical structures and synthetic pathway of the five chiral emitters named **Ax**-*p*-**CN**, **Ax**-*o*-**CHO**, **Hel**-*o*-**CN**, **Hel**-*p*-**CN** and **Hel**-*o*-**CHO** are depicted in Scheme 1. These compounds have been prepared following a convergent synthetic strategy, involving the bicarbazole system, BICOL, as the key intermediate. The latter was synthesized following our recently revisited procedure under its racemic form,[9a,17] implying firstly the preparation of 3-hydroxy carbazole, CBzOH, and an oxidative homocoupling reaction using vanadium complex as catalyst to afford 4,4'-bicarbazole-3,3'-diol, BICOL, derivative in 50% of yield. At this stage, BICOL was either alkylated at both the nitrogen and the oxygen positions to give *rac*-**Ax1**, or the two hydroxyl groups were bridged using diiodomethane in 90% yield before performing the alkylation at the two nitrogen atoms to afford *rac*-**Hel1**. Further iodination of these two intermediates, followed by Suzuki coupling reaction with the corresponding boronic acid derivatives, afforded the novel chiral donor-acceptor emitters in modest to good yield (up to 89 %, Scheme 1 and see the Electronic Supporting Information, ESI for details). Finally, the different derivatives with ee's up to 99% were obtained in enantiopure forms by HPLC separations over chiral stationary phases (see Supporting Information, ESI).

X-ray structure analyses of *rac*-**Ax**-*o*-**CHO**, which crystallized in the *P*-1 space group, provide further structural insights (Scheme 1). As expected, a dihedral angle of 106.6° between the carbazole units was measured, which indicates a weak electronic coupling between these two units. A second torsion angle of 43.3° is also measured between the carbazole and the benzaldehyde systems, suggesting again a moderate electronic interaction between the electron donor and accepting parts of the molecule, a prerequisite for obtaining TADF property. The aldehyde group does not point towards the opposite carbazole system but rather in direction of the methoxy group, thanks to the formation of two intramolecular hydrogen bonds with measured distances of 2.5 and 3.5 ångströms. Interestingly, the through-space interaction between the aldehyde group and the opposite carbazole unit can be also probed by the ^{1}H NMR spectra of both **Ax**-*o*-**CHO** and **Hel**-*o*-**CHO**. In comparison to a model monocarbazole-*o*-**CHO**, the aldehydic proton H_{Ald} appears much more shielded by almost 1 ppm for both bicarbazole based compounds, (Figure S1), owing to the current ring effect coming from the opposite π-conjugated carbazole system. The full experimental conditions and characterization (NMR and mass spectrometry) of all compounds are detailed in the SI.

ARTICLE

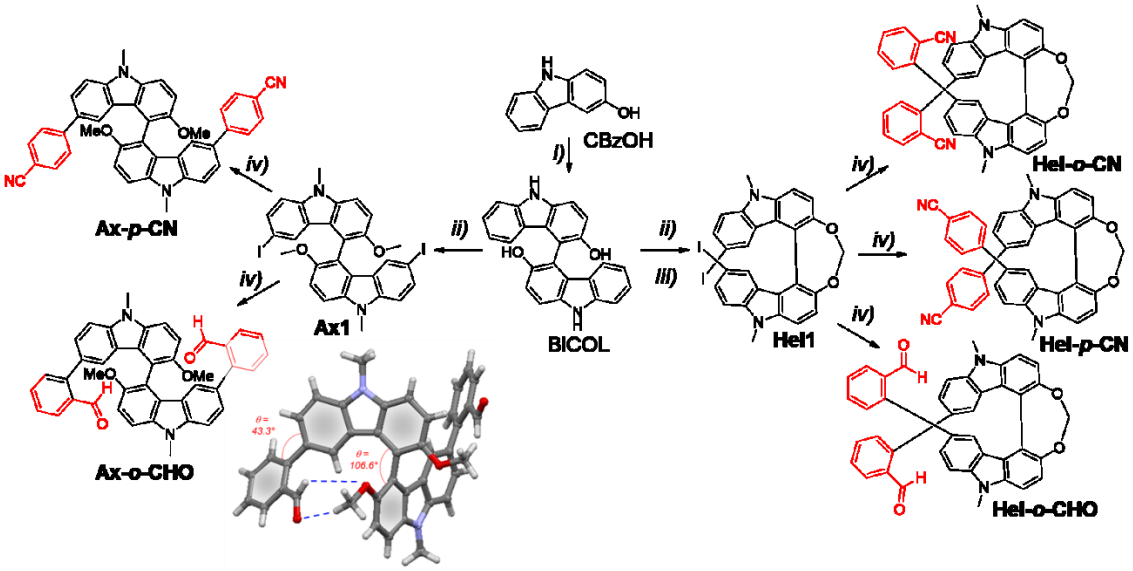

Scheme 1. Synthetic pathway to the chiral donor-acceptor emitters **Ax**-*p*-**CN**, **Ax**-*o*-**CHO**, **Hel**-*o*-**CN**, **Hel**-*p*-**CN** and **Hel**-*o*-**CHO**. Reaction conditions: (i) $VO(acac)_2$, MeCN, O_2, rt, 50%; (ii) Me_2SO_4, 22M NaOH, Acetone, Ar, reflux, 70%; (iii) BBr_3, DCM, rt, then CH_2I_2, K_2CO_3, acetone, Ar, reflux, 90% (over two steps); (iv) Suzuki coupling reaction involving the corresponding boronic acid partners (see SI for details). ORTEP drawing of **Ax**-o-**CHO** with 50% thermal ellipsoids. Further details are reported in SI.

Computational details

Computations were performed with Kohn-Sham Density functional theory (DFT) as implemented in the Gaussian (G16) package,[18] using the PBE0 functional[19] and the def2-SV(P) basis.[20]

Absorption and electronic circular dichroism (ECD) spectra were determined from the lowest 200 calculated vertical singlet electronic excitations. The spectra were Gaussian broadened with σ = 0.20 eV. Solvent effects on the spectra were considered by means of the polarizable continuum model (PCM) for toluene and dimethylformamide to match the experimental conditions.[21] 'D3' dispersion corrections were considered in the structure optimizations.[22] For overviews of the theoretical approach to model natural optical activity by quantum chemical calculations, in particular with TD-DFT, see, for example, available reviews.[23] Additional computational details, along with the full set of theoretical results, are provided in the ESI.

Ground-state photophysical and chiroptical properties

The UV-vis spectra of the novel chiral molecules were recorded in toluene solutions and compared to their axial and helical donor precursors (Figures 2 & S2). All the compounds bearing an *ortho*-substituted electron withdrawing group regarding the carbazole units (**Ax**-*o*-**CHO**, **Hel**-*o*-**CN** and **Hel**-*o*-**CHO**) display almost similar spectra with an intense transition found around 300-310 nm (ε between 35 and 45 $\times$ 10^3 M^{-1} cm^{-1}) and a low-energy pattern between 330 and 400 nm, constituted of several transitions with modest intensity (ε ~ 1.0 $\times$ 10^4 M^{-1} cm^{-1}, Figure 2). These optical signatures are closed to the ones recorded for their corresponding bicarbazole precursors, but significantly red-shifted by 15-20 nm in the low-energy part of the spectrum, indicating the presence of new charge-transfer (CT) transitions from the carbazole to the aldehyde and cyano units. This (CT) process is however of rather weak intensity, presumably due to the significant torsion angle between the donor and acceptor aromatic rings, as mentioned above for **Ax**-*o*-**CHO** (43.3°, Scheme 1). This is also confirmed by looking at the UV-vis spectra of **Hel**-*p*-**CN** and **Ax**-*p*-**CN**, which show a second broad absorption band centered at 330 and 345 nm, respectively, in place of the low intense signature found in the *ortho*-derivatives, still distinguishable for **Hel**-*p*-**CN** at 380 nm. This difference arises from the *para*-substitution of the electron withdrawing groups, which induces a stronger overlap of the donor and acceptor molecular orbitals, and therefore a stronger oscillator strength of the charge-transfer transition. Interestingly, going from helical bicarbazole donor to axial one seems to increase the intensity of the observed charge-transfer since the onset of the lowest absorption band is more red-shifted and with higher intensity for **Ax**-*p*-**CN** in comparison to **Hel**-*p*-**CN**. This result can be explained by the more electron donating strength of the axial bicarbazole system in comparison to the helical one, which has notably been explained for helical and axial bicarbazole precursors by the difference of torsion angle between the carbazole systems and the negative inductive effect play by the carbazolyl fragment (whose strength is dependent on the electronic interaction between the two carbazole units, see Figure S1).[9a] This remains also the case for the novel chiral compounds reported here, as evidenced by electrochemical experiments which afforded an oxidation potential of *ca.* 1 V *vs* ECS for the axial derivatives and around 1.2 V *vs* saturated calomel electrode (SCE) for the helical ones (see Table S2).

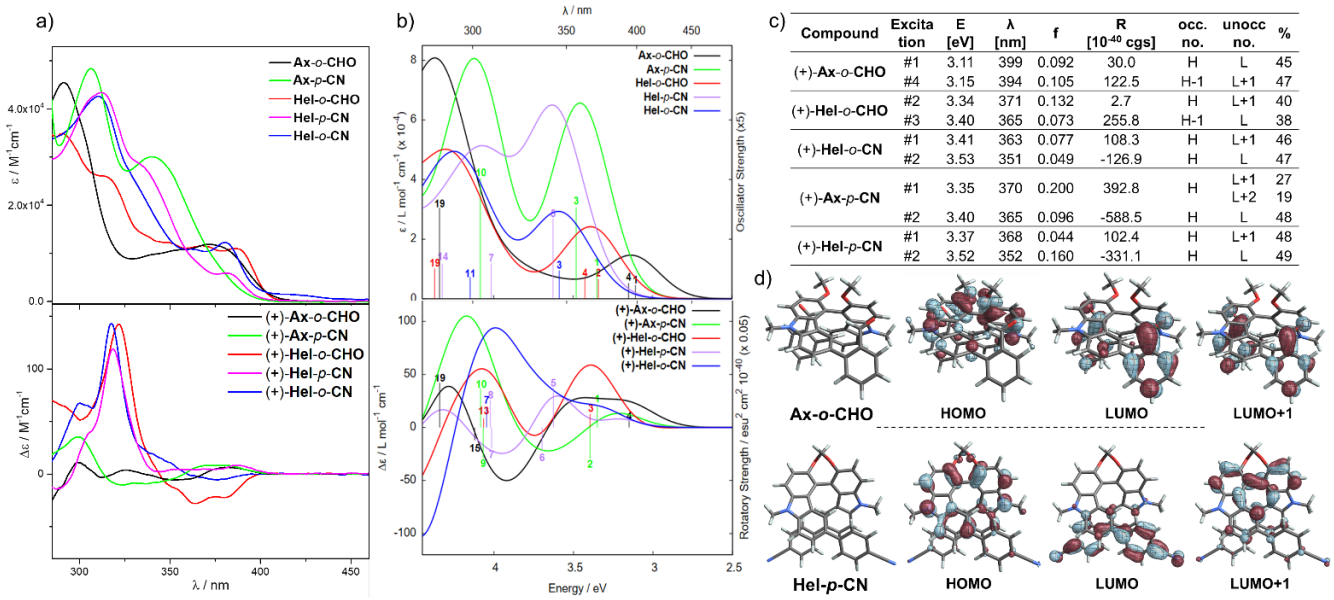

Compound	Excitation	E [eV]	λ [nm]	f	R [10^{-40} cgs]	occ. no.	unocc no.	%
(+)-**Ax**-*o*-**CHO**	#1	3.11	399	0.092	30.0	H	L	45
	#4	3.15	394	0.105	122.5	H-1	L+1	47
(+)-**Hel**-*o*-**CHO**	#2	3.34	371	0.132	2.7	H	L+1	40
	#3	3.40	365	0.073	255.8	H-1	L	38
(+)-**Hel**-*o*-**CN**	#1	3.41	363	0.077	108.3	H	L+1	46
	#2	3.53	351	0.049	-126.9	H	L	47
(+)-**Ax**-*p*-**CN**	#1	3.35	370	0.200	392.8	H	L+1 L+2	27 19
	#2	3.40	365	0.096	-588.5	H	L	48
(+)-**Hel**-*p*-**CN**	#1	3.37	368	0.044	102.4	H	L+1	48
	#2	3.52	352	0.160	-331.1	H	L	49

Figure 2. Experimental a) and calculated b) UV-vis (top) and ECD (bottom) spectra of **Ax**-*o*-**CHO** (black), **Ax**-*p*-**CN** (green), **Hel**-*o*-**CHO** (red), **Hel**-*p*-**CN** (purple) and **Hel**-*o*-**CN** (blue) measured in toluene at 298 K (~10^{-5} M). For the calculated spectra, selected transitions and oscillator and rotatory strengths are indicated as 'stick bars', and detailed in table c), with oscillator and rotatory strengths; d) Isosurfaces (±0.04 au) of the frontier molecular orbitals (MOs) for (+)-**Ax**-*o*-**CHO** and (+)-**Hel**-*p*-**CN**.

Theoretical calculations bring further insights regarding the obtained optical properties. As expected, for all compounds the HOMOs are delocalized over the two carbazole units, while the LUMOs are found on the aryl-CHO and aryl-CN acceptors (Figure 2), confirming the push-pull nature of the chromophores. In each case, the LUMO and LUMO+1 levels are found to be quasi-degenerate, separated by no more than 0.060 eV. For all compounds, the HOMO and HOMO-1 are seen to be +/- linear combinations of fragment orbitals of the two different carbazole parts, with energy differences ranging from 0.060 eV for **Ax**-*o*-**CHO** to around 0.150 eV for the other compounds. For **Ax**-*o*-**CHO**, Fig. 2 shows that LUMO and LUMO+1, likewise, are +/- linear combinations of fragment orbitals in the acceptor moieties. For **Hel**-*p*-**CN** (and **Hel**-*o*-**CN**), the +/- linear combinations are LUMO and LUMO+2 instead, with LUMO+2 also being energetically nearly degenerate with LUMO. The lowest-energy excitations with sizeable oscillator strength (*f*) correspond to HOMO-LUMO and HOMO-LUMO+1/2 transitions ranging from 363 and 400 nm for **Hel**-*o*-**CN** and **Ax**-***o***-**CHO** respectively, with for the latter the involvement of HOMO-1 as well. While the LUMO and LUMO+1 levels are delocalized on the electron-withdrawing groups for **Ax**-*p*-**CN**, **Ax**-*o*-**CHO** and **Hel**-*o*-**CHO**, the LUMO+1 is delocalized over the entire bicarbazole system for **Hel**-*p*-**CN** and **Hel**-*o*-**CN**, which indicates a weaker transition dipole moment for these compounds owing to both the less electron donor character of the helical carbazole unit combined to the less electron withdrawing effect of the cyano-aryl groups.

Electronic circular dichroism (ECD) of the investigated compounds further highlights differences between the axial and helical donor-acceptor compounds. The obtained spectra for (+)-**Ax**-*p*-**CN** and (+)-**Ax**-*o*-**CHO** in toluene solution appear similar in the high energy region with an intense positive band around 280-300 nm. While (+)-**Ax**-*p*-**CN** displays in the low-energy region only one set of negative and positive signals at 330 and 380 nm, respectively, the signature of (+)-**Ax**-*o*-**CHO** shows four distinct bands at 310, 328, 360 and 380 nm of successively negative and positive signs. Regarding (+)-**Hel**-*p*-**CN**, (+)-**Hel**-*o*-**CN** and (+)-**Hel**-*o*-**CHO**, their ECD spectra are composed of one intense band at 320 nm, followed by a broad positive one between 340 and 410 nm for the former, but a negative signal at 375 nm for the two latter, highlighting an impact on the substituted position of the electron withdrawing group.

The calculated ECD spectra for the (+)-**Ax** compounds better agree with experiments than for the (+)-**Hel** systems (Figure 2). The following discussion is for the (+) enantiomers. For all compounds, two positive and one negative bands with distinct intensities appear in the calculated ECD spectra. The qualitative assignment of the ECD bands for **Ax**-*o*-**CHO** and **Hel**-*o*-**CHO**, from low to high energy, is as follows: intramolecular charge transfer (ICT), ICT and $\pi \rightarrow \pi^*$ excitations, for **Ax**-*p*-**CN** and **Hel**-*o*-**CN**, the three bands present a combination of ICT and $\pi \rightarrow \pi^*$ excitations, and for **Hel**-*p*-**CN** is a combination of ICT and $\pi \rightarrow \pi^*$ excitations, ICT and $\pi \rightarrow \pi^*$ excitations. In general, the transitions with large *f* also have large rotatory strengths (*R*). For (+)-**Ax** compounds, the lowest-energy band is weak and positive due to ICT excitations from the HOMO-1 to LUMO+1 for **Ax**-*o*-**CHO** and HOMO to LUMO+1 for **Ax**-*p*-**CN**. The following negative band at 3.9 eV (318 nm) for **Ax**-*o*-**CHO** and 3.6 eV for **Ax**-*p*-**CN** is caused by ICT excitations from the HOMO. Although each **Ax**-system shows a positive band at above 4 eV (310 nm), the excitation that causes the band corresponds to $\pi \rightarrow \pi^*$ transitions for **Ax**-*o*-**CHO** and ICT for **Ax**-*p*-**CN**. We note that the increase of the long-wavelength positive band at around 390 nm and negative band at around 340 nm for **Ax**-*p*-**CN**, as well as the large rotatory strengths of the first excitations, suggest the presence of exciton coupling between the electric transition dipoles of the carbazole fragments. For **Hel**-*o*-**CHO** and **Hel**-*p*-**CN**, the first longest-wavelength positive ECD band is attributed to the HOMO-1 to LUMO transition. Although the qualitative assignment for the ECD band at around 300-310 nm

is the same for both **Hel**-*o*-**CHO** and **Hel**-*p*-**CN**, they show opposite signs; positive for **Hel**-*o*-**CHO** and negative for **Hel**-*p*-**CN**. Different from these systems, the **Hel**-*o*-**CN** shows a broad positive band mainly caused by $\pi \rightarrow \pi^*$ excitations.

Excited-state photophysical and chiroptical properties

The unpolarized luminescence spectra of the chiral emitters have been firstly recorded in toluene solutions and are depicted in Figure 3. In this weakly polar solvent, all the compounds exhibit a structured luminescence spectrum between 400 and 500 nm, except **Ax**-*o*-**CHO**, which display a broad and red-shifted emission profile with a maximum at 460 nm owing to the higher charge-transfer character of its excited-state. Going to more polar solvents such as chloroform and dimethylformamide impacts significantly the luminescence maxima of **Ax**-*p*-**CN**, **Ax**-*p*-**CHO** and **Hel**-*p*-**CHO**, with a red-shift of their emission bands (Table S1 and Figures S3-S5), while the emission spectra of **Hel**-*p*-**CN** and **Hel**-*o*-**CN** remain almost not affected. This solvatochromism effect is more pronounced for **Ax**-*p*-**CHO** and **Hel**-*p*-**CHO**, which show maxima of luminescence at 500 and 560 nm, respectively, in dimethylformamide, due to the stronger electron withdrawing character of the aldehyde group in comparison to the cyano one.

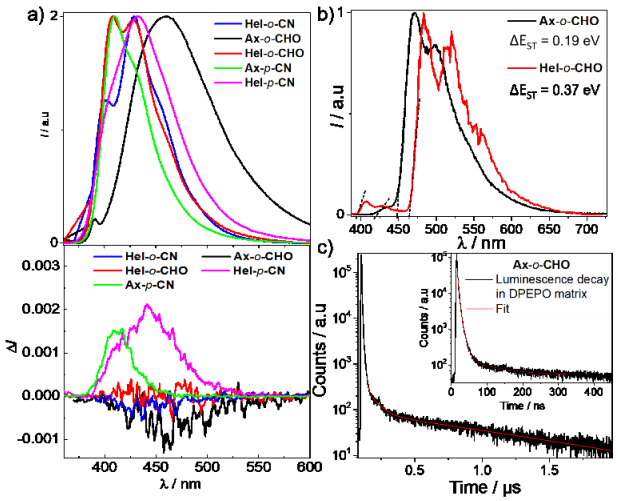

Figure 3. a) Luminescence and CPL spectra of (+)-**Ax**-*p*-**CN** (green), (+)-**Ax**-*o*-**CHO** (black), (+)-**Hel**-*o*-**CN** (blue), (+)-**Hel**-*p*-**CN** (purple) and (+)-**Hel**-*o*-**CHO** (red) measured in toluene at 298 K (~10^{-5} M); b) Luminescence spectra of (+)-**Ax**-*o*-**CHO** (black) and (+)-**Hel**-*o*-**CHO** (red) recorded at 77 K (with estimated values of the singlet (S)-triplet (T) energy gap; c) Luminescence decays of (+)-**Ax**-*o*-**CHO** (black signal, corresponding fits in red) recording under vacuum in solid matrix (bis[2-(diphenylphosphino)phenyl] ether oxide, DPEPO) with an inset focusing on the short lifetime decays.

Further photophysical characterizations of **Ax**-*p*-**CHO** and **Hel**-*p*-**CHO** show a decrease of their emission intensity in presence of oxygen in chloroform solution, suggesting TADF property. Careful evaluation of their photoluminescence lifetimes in bis[2-(diphenylphosphino)phenyl] ether oxide (DPEPO) matrix, in the absence of oxygen, reveals the presence of a long lifetime with a decay of 1.04 and 0.80 μs for **Ax**-*p*-**CHO** and **Hel**-*p*-**CHO**, respectively (Figure 3 and S1), confirming the TADF property of these chiral emitters. We therefore evaluate the ΔE_{ST} of these emitters by recording their luminescence spectra at 77 K, which show a structured phosphorescence emission with an onset at 450 and 465 nm for **Ax**-*p*-**CHO** and **Hel**-*p*-**CHO**, respectively, resulted in corresponding T_1 energy levels of 2.76 and 2.67 eV. A residual fluorescence signal can be also identified for both compounds and help us to estimate their S_1 energy levels from the onset of the emission band, of 2.95 and 3.06 eV for **Ax**-*p*-**CHO** and **Hel**-*p*-**CHO**, respectively, which result in corresponding ΔE_{ST} values of 0.190 and 0.370 eV. While the obtained S-T gap of the axial emitter is in the classical range found for TADF emitters, the one for the helical one is relatively high and may explain the two times smaller TADF efficiency for **Hel**-*p*-**CHO** (ϕ_{TADF} = 5%), in comparison to **Ax**-*p*-**CHO** (ϕ_{TADF} = 10%). This finding further highlights the influence of the torsion angle between the two carbazole systems in this photophysical process, where a higher electronic communication (lower torsion angle) between the carbazole units in the helical derivative appears detrimental to reach a small ΔE_{ST}, (*i.e.* lower than 0.300 eV). The other compounds based on cyano acceptor units do not show any TADF property, owing probably to their significant ΔE_{ST}, of more than 0.50 eV (see SI).

Mirror-image CPL spectra were obtained in toluene solution for the five emitters (Figure S11), with maxima corresponding to the unpolarized spectra, and intensity in the range of classical chiral organic emitters (g_{lum} ~ 10^{-3}),[1c,3a,16c] as depicted in Figure 3 for the (+) enantiomers. Among all, compounds (+)-**Ax**-*p*-**CN** and (+)-**Hel**-*p*-**CN** display the highest CPL intensity, with g_{lum} values of + 1.5 and + 2.0 × 10^{-3}, respectively, while (+)-**Ax**-*o*-**CHO** and (+)-**Hel**-*o*-**CN** show g_{lum} of - 1.0 × 10^{-3} and - 0.5 × 10^{-4}, respectively. All these values are consistent with the absorption dissymmetry factors g_{abs}, measured at the lowest energy transition (Table S1),[16c] indicating that both ground and emitting excited states have a similar chiral geometry in toluene. Surprisingly, and despite its intense ECD low energy band, (+)-**Hel**-*o*-**CHO** shows no clear distinguishable CPL signal. To get further insights on these responses and giving our recent results on CPL solvatochroism,[14c,24] we therefore investigated the CPL of the five emitters in chloroform and dimethylformamide. As expected, the maxima of CPL follow the red-shifted ones observed for unpolarized luminescence in both solvents for all the compounds. While (+)-**Ax**-*p*-**CN** and (+)-**Ax**-*o*-**CHO** display a decrease of g_{lum} values when polarity increases, as previously observed for several systems,[8b,c,g,14c,24] (+)-**Hel**-*p*-**CN** and (+)-**Hel**-*o*-**CHO** show a significant increase of CPL intensity when going to chloroform and dimethylformamide solvents, with g_{lum} values reaching up to 2.6 × 10^{-3} and 2.0 × 10^{-3} for the cyano and aldehyde helical emitters, respectively (Figure 4).

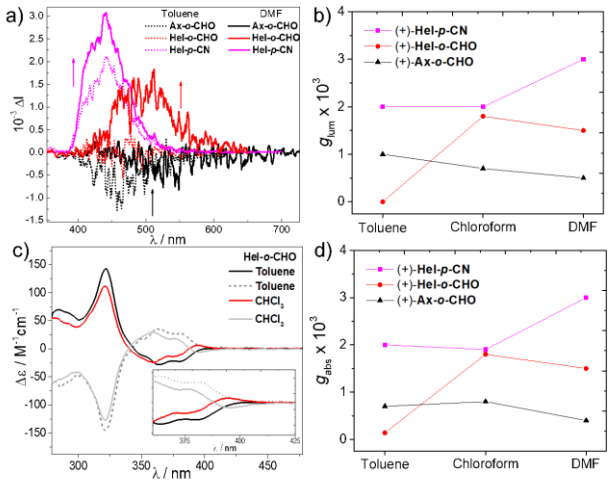

Figure 4. a) CPL spectra of (+)-**Ax**-*o*-**CHO** (black), (+)-**Hel**-*p*-**CN** (purple) and (+)-**Hel**-*o*-**CHO** (red) measured in toluene (dotted lines) and in dimethylformamide (solid lines) at 298 K (~10^{-5} M); b) Corresponding luminescence dissymmetry factor values for (+)-**Ax**-*o*-**CHO** (black), (+)-**Hel**-*p*-**CN** (purple) and (+)-**Hel**-*o*-**CHO** (red) measured in toluene, chloroform and in dimethylformamide at 298 K (~10^{-5} M); c) ECD spectra of (+)-**Ax**-*o*-**CHO** measured in toluene (black solid line) and in dimethylformamide (red solid line) with their corresponding enantiomers in grey at 298 K (~10^{-5} M); d) Absorption dissymmetry factor values for (+)-**Ax**-*o*-**CHO** (black), (+)-**Hel**-*p*-**CN** (purple) and (+)-**Hel**-*o*-**CHO** (red) measured in toluene, chloroform and in dimethylformamide at 298 K (~10^{-5} M).

This unexpected difference of behavior between axial and helical emitters is really surprising and only few examples have reported an increase (or even a sign inversion) of CPL when going to a more polar solvent,[8a,25] attributed to either a dual-fluorescence behavior,[8b] a change in the molecular conformation change,[8f] or a modulation of the involved transition(s) in the emission process.[8c,g,26]

In the present case, it is interesting to note that for (+)-**Hel**-*o*-**CHO** and (+)-**Hel**-*p*-**CN** the intensity of both ECD and CPL are changing when going from toluene to dichloromethane and dimethylformamide. Indeed, comparing the corresponding g_{abs} values of the low energy transition and the g_{lum} indicate that both ground- and excited-states chirality are impacted by the polarity of the solvent (Figure 4). This is notably clearly identified for (+)-**Hel**-*o*-**CHO**, which exhibits a different low energy ECD pattern in both chloroform and dimethylformamide than in toluene, with the appearance of a positive contribution at 395 nm. This significant change in the ECD indicates either structural changes leading to a different conformer in more polar solvent (orientation of the aldehyde groups towards the carbazole units), or a reorganization of the orbital frontiers within the donor-acceptor structure with increasing solvent polarity. Since no red-shift is observed in both UV-vis and ECD spectra and no obvious structural change has been observed either experimentally (^{1}H NMR spectra in toluene and chloroform are rather similar, Figure S1), nor theoretically (see the comparison of the optimized molecular structures obtained in toluene and dimethylformamide in Figure S36-37), we therefore exclude the presence of different structural conformers in solution. This is confirmed by the fact that the increase of ECD and CPL intensities also happens for (+)-**Hel**-*p*-**CN**, which has only one possible conformer due the *para* substitution of the cyano functional group.

We therefore surmise that the stronger electrostatic field imposed by the polar solvents induces a modulation of the intramolecular charge transfer transitions between the bicarbazole system and the phenyl aldehyde substituents. In fact, the rather limited electronic interaction between the two carbazole units (torsion angle of more than 50° between the two π-systems) and the positive/negative low energy ECD signature suggest the presence of exciton coupling between two carbazole→Phenyl-Aldehyde transitions in chloroform and dimethylformamide, which creates strong magnetic transition dipoles that are not perpendicular to the coupled electric transition dipoles.

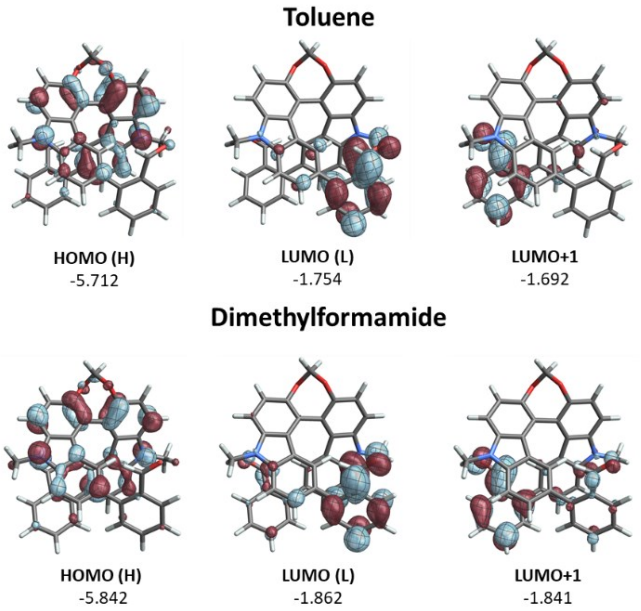

Figure 5. Isosurfaces (±0.04 au) of frontier Molecular Orbitals (MOs) for (+)-**Hel**-*o*-**CHO** in toluene (up) and dimethylformamide (down) with their corresponding orbitals energies in eV.

Excitation	E [eV]	λ [nm]	f	R [10^{-40} cgs]	occ. no.	unocc no.	%
Toluene							
#1	3.237	383	0.014	-33.0	H	L	47
#2	3.341	371	0.132	2.69	H	L+1	40
DMF							
#1	3.277	378	0.020	-84.16	H	L L+1	26 20
#2	3.329	372	0.148	119.22	H	L+1 L	26 17

Table 1. First sizeable excitations and occupied (occ)-unoccupied (unocc) MO pair contributions (greater than 10%) for (+)-**Hel**-*o*-**CHO** in toluene and dimethylformamide.

Visual comparison of the isosurfaces of the frontier molecular orbitals in toluene and dimethylformamide show that the HOMO seems equally delocalized over the two carbazole units for both solvents (Figure 5). In addition, the LUMO and LUMO+1, on each phenyl-aldehyde substituent, appear more degenerate in dimethylformamide, separated by 0.021 eV (0.062 eV in toluene). Finally, theoretical calculations show that the lowest energy excitation of (+)-**Hel**-*o*-**CHO** in dimethylformamide, excitation n°1 at 378 nm (Table 1), implies the HOMO to LUMO and HOMO to

LUMO+1 transitions, a different scenario than in toluene where the lowest energy excitation is mainly attributed to the HOMO to LUMO transition (the HOMO-LUMO+1 transition appears higher in energy by 0.100 eV, see Table 1).

This situation in dimethylformamide is reminiscent to the one we previously faced for π-helical push-pull systems based on carbo[6]helicene, which acts as a chiral electron donor unit and mediates an intramolecular chiral exciton coupling between the electric transition dipoles involving electron-withdrawing groups within the helical environment.[14c,24,27] However, while this exciton coupling is a major contributor to the obtained strong ECD and CPL responses for helicene based dyes, its intensity strongly decreases upon polarity increase, especially for the CPL signal.[14c,24] In the investigated bicarbazole chiral systems here, we observe a completely reverse process since polarity triggers the increase of ECD and CPL responses by promoting two *quasi*-degenerate charge-transfer electronic transitions involving one helical (non-fully conjugated) chiral donor. Moreover, the sign of the resulting exciton CD couplet is consistent with the sense of the helical arrangement of the coupled electric transition dipole moments, *i.e.* a positive exciton coupling signature for the (*S*)-**Hel**-*o*-**CHO**, and *vice versa*.[28]

A similar process also occurs for (+)-**Hel**-*p*-**CN** with an increase of CPL intensity by 50% in dimethylformamide (Figure 4), and a less obvious change in its ECD response, albeit with a slight but distinct positive/negative low energy response around 350 nm, not observed for toluene and chloroform solvents (Figure S15). Theoretical calculations reveal that the HOMO of (+)-**Hel**-*p*-**CN** is already equally delocalized over the two carbazole units in toluene, and that the lowest energy excitation of (+)-**Hel**-*p*-**CN**, excitation n°1 at 368 nm (Figure 2), acquires a more charge-transfer character in dimethylformamide in comparison to the one calculated in toluene, which is almost exclusively localized on the bicarbazole systems. These findings are in line with the obtained results for (+)-**Hel**-*o*-**CHO** and the weaker difference of ECD and CPL increase observed for (+)-**Hel**-*p*-**CN** may be related to the weaker electron accepting ability of the cyano substituent in comparison to the aldehyde one in (+)-**Hel**-*o*-**CHO**. This results in less intense charge-transfer character of the involved electronic transitions, as evidenced by the visual comparison of the LUMO and LUMO+1 of both compounds (Figure S37 & S45). This also explain why we do not see such intensity increase of the chiroptical properties for (+)-**Hel**-*o*-**CN**, since the corresponding lowest energy excitation is mainly localized on the bicarbazole systems (Table S6 and Figure S40). Based on these findings, we can tentatively explain why (+)-**Hel**-*o*-**CHO** emitter does not display clear CPL signal in toluene solution. Indeed, both (+)-**Hel**-*o*-**CHO** and (+)-**Hel**-*o*-**CN** compounds show a structured signature in toluene with a slight red-shift observed for (+)-**Hel**-*o*-**CHO**, owing to the stronger withdrawing effect of the aldehyde substituent in comparison to the cyano one. Accordingly, while (+)-**Hel**-*o*-**CN** presents an excited-state almost independent of the polarity of solvent and probably significantly localized on the helical donor unit, (+)-**Hel**-*o*-**CHO** may present an interplay of locally and charge-transfer excited-state characters, both contributing to the overall CPL signature in toluene. Since the CPL signature observed for (+)-**Hel**-*o*-**CN** presents a negative and rather weak glum value of - 0.5 × 10^{-3} in this solvent, one can think that this contribution for (+)-**Hel**-*o*-**CHO** is counteracted by the charge-transfer transition, responsible of the positive CPL values in dichloromethane and dimethylformamide solvents, which reach glum values of more than + 1.5 × 10^{-3}. For the axial derivatives, (+)-**Ax**-*o*-**CHO** and (+)-**Ax**-*p*-**CN**, the lower ECD and CPL intensities come presumably because of the torsion angle of nearly 90° between the two electronic dipoles, as already observed for the axial bicarbazole precursors,[9a] and in close analogy with binaphthyl and helicene like systems.[28a,29] Finally, it is worth to note that the other reported systems presenting CPL sign inversion in function of the polarity display also two electronically connected D-A dipoles in a helically chiral environment,[8b,c] emphasizing some key molecular designs for reaching CPL switchable materials by intramolecular charge-transfer dynamics.[8a,25]

Conclusions

In conclusion, we described here the synthesis of new axially and helically chiral donor-acceptor emitters and investigated both experimentally and theoretically their chiroptical properties. We showed that CP-TADF can be obtained when both axial and helical bicarbazole systems are functionalized with carbonyl-based accepting groups, and that the efficiency of the TADF process is dependent on the torsion angle between the two carbazole systems, which directly impacts the donor strength of the chiral donor unit. Interestingly, the obtained CPL for the axial and helical emitters shows an opposite modulation in function of the polarity of the solvent, with notably a strong increase of the luminescence dissymmetry factor, g_{lum}, from 0 to 2 × 10^{-3} for **Hel**-*o*-**CHO**. We attributed this switch of CPL to a subtle reorganization of the intramolecular charge-transfer dynamics in both ground- and excited-states as evidenced by experimental and theoretical experiences. Although it rather hard to find a direct correlation between CPL and TADF, especially because the latter also involves triplet excited states, our results suggest that a higher CPL intensity can be found for helical compounds, among which, Hel-o-CHO displays TADF but with a lower efficiency in comparison to Ax-o-CHO. This has been explained, in part, by the lower donor strength of the helical bicarbazole system, which ultimately leads to higher ΔE_{ST}. While the use of an electron withdrawing acceptor of significant intensity in a *ortho*-substitution pattern is crucial for reaching the TADF property, clearly the chiral donor fragment, based here on two carbazole units, is important for modulating both the TADF and the CPL efficiencies. Further works regarding a deeper rationalization of these aspects are currently under investigations in our laboratory and rely on the molecular engineering of the chiral part to ultimately favor smaller ΔE_{ST} for helical based CP-TADF emitters. We hope that this relationship-structure property investigation may offer new opportunities to design innovative and efficient CPL emitters.

Conflicts of interest

There are no conflicts to declare.

Acknowledgements

We acknowledge the Ministère de l'Education Nationale, de la Recherche et de la Technologie, the Centre National de la Recherche Scientifique (CNRS) and the French National Research Agency (ANR) for financial support (iChiralight project, ANR-19-CE07-0040). J. A. thanks the National Science Foundation (CHE-1855470) for financial support of the theoretical component of this study, and the Center for Computational Research (CCR) at the University at Buffalo,[30] http://hdl.handle.net/10477/79221, for computational resources. The PRISM core facility (Biogenouest©, UMS Biosit, Universitéd de Rennes 1 – Campus de Villejean – 35043 RENNES Cedex, France) is acknowledged for the NMR characterizations and ECD measurements.

Notes and references

1 a) M. Lindemann, G. Xu, T. Pusch, R. Michalzik, M. R. Hofmann, I. Žutić and N. C. Gerhardt, *Nature*, 2019, **568**, 212-215; b) H. Wang, L. liu and C. Lu, *Procedia Comput. Sci.*, 2018, **131**, 511-519; c) J. M. Han, S. Guo, H. Lu, S. J. Liu, Q. Zhao and W. Huang, *Adv. Opt. Mater.*, 2018, **6**, 1800538; d) T. Novikova, A. Pierangelo, S. Manhas, A. Benali, P. Validire, B. Gayet and A. D. Martino, *Appl. Phys. Lett.*, 2013, **102**, 241103; e) B. Kunnen, C. Macdonald, A. Doronin, S. Jacques, M. Eccles and I. Meglinski, *J. Biophotnics*, 2015, **8**, 317-323; f) R. Carr, N. H. Evans and D. Parker, *Chem. Soc. Rev.*, 2012, **41**, 7673-7686.

2 a) F. Zinna and L. Di Bari, *Chirality*, 2015, **27**, 1-13; b) E. R. Neil and D. Parker, *RSC Advances*, 2017, **7**, 4531-4540; c) S. Shuvaev, M. A. Fox and D. Parker, *Angew. Chem. Int. Ed.*, 2018, **57**, 7488-7492; d) F. Zinna, M. Pasini, F. Galeotti, C. Botta, L. Di Bari and U. Giovanella, *Adv. Funct. Mater.*, 2017, **27**, 1603719; e) J.-R. Jiménez, B. Doistau, C. M. Cruz, C. Besnard, J. M. Cuerva, A. G. Campaña and C. Piguet, *J. Am. Chem. Soc.*, 2019, **141**, 13244-13252; f) J. R. Jimenez, M. Poncet, S. Miguez-Lago, S. Grass, J. Lacour, C. Besnard, J. M. Cuerva, A. G. Campana and C. Piguet, *Angew. Chem. Int. Ed. Engl.*, 2021, **60**, 10095-10102.

3 a) L. Arrico, L. Di Bari and F. Zinna, *Chem. Eur. J.*, 2021, **27**, 2920-2934; b) Y. Nagata and T. Mori, *Front. Chem.*, 2020, **8**.

4 a) J. Gilot, R. Abbel, G. Lakhwani, E. W. Meijer, A. P. H. J. Schenning and S. C. J. Meskers, *Adv. Mater.*, 2010, **22**, E131-E134; b) Y. Yang, R. C. da Costa, M. J. Fuchter and A. J. Campbell, *Nat Photon*, 2013, **7**, 634-638; c) Y. Yang, R. C. da Costa, D.-M. Smilgies, A. J. Campbell and M. J. Fuchter, *Adv. Mater.*, 2013, **25**, 2624-2628; d) J. R. Brandt, X. Wang, Y. Yang, A. J. Campbell and M. J. Fuchter, *J. Am. Chem. Soc.*, 2016, **138**, 9743-9746; e) S. Feuillastre, M. Pauton, L. Gao, A. Desmarchelier, A. J. Riives, D. Prim, D. Tondelier, B. Geffroy, G. Muller, G. Clavier and G. Pieters, *J. Am. Chem. Soc.*, 2016, **138**, 3990-3993; f) M. Schulz, M. Mack, O. Kolloge, A. Lutzen and M. Schiek, *Phys. Chem. Chem. Phys.*, 2017, **19**, 6996-7008; g) P. Josse, L. Favereau, C. Shen, S. Dabos-Seignon, P. Blanchard, C. Cabanetos and J. Crassous, *Chem. Eur. J.*, 2017, **23**, 6277-6281; h) J. R. Brandt, F. Salerno and M. J. Fuchter, *Nat. Rev. Chem.*, 2017, **1**, 0045.

5 a) J. Wade, J. R. Brandt, D. Reger, F. Zinna, K. Y. Amsharov, N. Jux, D. L. Andrews and M. J. Fuchter, *Angew Chem Int Ed* 2021, **60**, 222-227; b) J. Greenfield, J. Wade, J. Brandt, X. Shi, T. Penfold and M. Fuchter, *Chem. Sci.*, 2021, DOI: 10.1039/D1SC02335G.

6 a) G. Longhi, E. Castiglioni, J. Koshoubu, G. Mazzeo and S. Abbate, *Chirality*, 2016, **28**, 696-707; b) H. Tanaka, M. Ikenosako, Y. Kato, M. Fujiki, Y. Inoue and T. Mori, *Commun. Chem.*, 2018, **1**, 38; c) C. Schaack, L. Arrico, E. Sidler, M. Gorecki, L. Di Bari and F. Diederich, *Chem. Eur. J.*, 2019, **25**, 8003-8007; d) Y. Liu, Q. Xu, J. Sun, L. Wang, D. He, M. Wang and C. Yang, *Spectrochimica Acta Part A: Molecular and Biomolecular Spectroscopy*, 2020, **239**, 118475; e) K. Tani, R. Imafuku, K. Miyanaga, M. E. Masaki, H. Kato, K. Hori, K. Kubono, M. Taneda, T. Harada, K. Goto, F. Tani and T. Mori, *J. Phys. Chem. A*, 2020, **124**, 2057-2063.

7 a) L. Frédéric, A. Desmarchelier, R. Plais, L. Lavnevich, G. Muller, C. Villafuerte, G. Clavier, E. Quesnel, B. Racine, S. Meunier-Della-Gatta, J. P. Dognon, P. Thuéry, J. Crassous, L. Favereau and G. Pieters, *Adv. Funct. Mater.*, 2020, **30**, 2004838; b) L. Frederic, A. Desmarchelier, L. Favereau and G. Pieters, *Adv. Funct. Mater.*, 2021, 2010281; c) M. Li, S. H. Li, D. Zhang, M. Cai, L. Duan, M. K. Fung and C. F. Chen, *Angew Chem Int Ed* 2018, **57**, 2889-2893; d) N. Sharma, E. Spuling, C. M. Mattern, W. Li, O. Fuhr, Y. Tsuchiya, C. Adachi, S. Brase, I. D. W. Samuel and E. Zysman-Colman, *Chem Sci*, 2019, **10**, 6689-6696; e) S. Sun, J. Wang, L. Chen, R. Chen, J. Jin, C. Chen, S. Chen, G. Xie, C. Zheng and W. Huang, *J. Mater. Chem. C*, 2019, **7**, 14511-14516; f) Z. G. Wu, H. B. Han, Z. P. Yan, X. F. Luo, Y. Wang, Y. X. Zheng, J. L. Zuo and Y. Pan, *Adv Mater*, 2019, **31**, e1900524; g) M. Li, Y. F. Wang, D. Zhang, L. Duan and C. F. Chen, *Angew. Chem. Int. Ed. Engl.*, 2020, **59**, 3500-3504; h) Z.-L. Tu, Z.-P. Yan, X. Liang, L. Chen, Z.-G. Wu, Y. Wang, Y.-X. Zheng, J.-L. Zuo and Y. Pan, *Adv. Sci.*, 2020, **7**, 2000804; i) Y. F. Wang, M. Li, W. L. Zhao, Y. F. Shen, H. Y. Lu and C. F. Chen, *Chem Commun* 2020, **56**, 9380-9383; j) S. Y. Yang, Y. K. Wang, C. C. Peng, Z. G. Wu, S. Yuan, Y. J. Yu, H. Li, T. T. Wang, H. C. Li, Y. X. Zheng, Z. Q. Jiang and L. S. Liao, *J. Am. Chem. Soc.*, 2020, **142**, 17756-17765; k) L. Zhou, G. Xie, F. Ni and C. Yang, *Appl. Phys. Lett.*, 2020, **117**, 130502; lE. Yen-Pon, F. Buttard, L. Frédéric, P. Thuéry, F. Taran, G. Pieters, P. A. Champagne and D. Audisio, *JACS Au*, 2021, DOI: 10.1021/jacsau.1c00084.

8 a) J.-L. Ma, Q. Peng and C.-H. Zhao, *Chem. Eur. J.*, 2019, **25**, 15441-15454; b) Z.-B. Sun, J.-K. Liu, D.-F. Yuan, Z.-H. Zhao, X.-Z. Zhu, D.-H. Liu, Q. Peng and C.-H. Zhao, *Angew. Chem. Int. Ed.*, 2019, **58**, 4840-4846; c) W.-B. Lin, D.-Q. He, H.-Y. Lu, Z.-Q. Hu and C.-F. Chen, *Chem. Commun.*, 2020, **56**, 1863-1866; d) M.-Y. Zhang, X. Liang, D.-N. Ni, D.-H. Liu, Q. Peng and C.-H. Zhao, *Org. Lett.*, 2021, **23**, 2-7; e) S. Nakanishi, N. Hara, N. Kuroda, N. Tajima, M. Fujiki and Y. Imai, *Org. Biomol. Chem.*, 2018, **16**, 1093-1100; f) K. Takaishi, K. Iwachido and T. Ema, *J. Am. Chem. Soc.*, 2020, **142**, 1774-1779; g) M.-Y. Zhang, X. Liang, D.-N. Ni, D.-H. Liu, Q. Peng and C.-H. Zhao, *Org. Lett.*, 2021, **23**, 2-7.

9 a) S. Kasemthaveechok, L. Abella, M. Jean, M. Cordier, T. Roisnel, N. Vanthuyne, T. Guizouarn, O. Cador, J. Autschbach, J. Crassous and L. Favereau, *J. Am. Chem. Soc.*, 2020, **142**, 20409-20418; b) R. Takishima, Y. Nishii and M. Miura, *Org. Lett.*, 2021, DOI: 10.1021/acs.orglett.1c00011.

10 P. Sumsalee, L. Abella, S. Kasemthaveechok, N. Vanthuyne, M. Cordier, G. Pieters, J. Autschbach, J. Crassous and L. Favereau, *submitted*, 2021, under review

11 Y.-F. Wang, H.-Y. Lu, C. Chen, M. Li and C.-F. Chen, *Org. Electron.*, 2019, **70**, 71-77.

12 a) B. Wex and B. R. Kaafarani, *J. Mater. Chem. C*, 2017, **5**, 8622-8653; b) M. Godumala, S. Choi, M. J. Cho and D. H. Choi, *J. Mater. Chem. C*, 2019, **7**, 2172-2198; c) Q. Wei, Z. Ge and B. Voit, *Macromol. Rapid Commun.*, 2019, **40**, 1800570; d) J.-M. Teng, Y.-F. Wang and C.-F. Chen, *J. Mater. Chem. C*, 2020, **8**, 11340-11353.

13 *TADF molecular materials based on a [5]-helicene core have been devlopped (see Takeda et al. Synthesis 2021, **53**, 1584 and Dias, Skabara et al. J. Mater. Chem. C, 2018, **6**, 10557) but their chiroptical properties have never been investigated.* .

14 a) W.-L. Zhao, M. Li, H.-Y. Lu and C.-F. Chen, *Chem. Commun.*, 2019, **55**, 13793-13803; b) J. Crassous, in *Circularly Polarized Luminescence of Isolated Small Organic Molecules*, ed. T. Mori, Springer Singapore, Singapore, 2020, DOI: 10.1007/978-981-15-2309-0_4, pp. 53-97; c) K. Dhbaibi, L. Abella, S. Meunier-Della-Gatta, T. Roisnel, N. Vanthuyne, B. Jamoussi, G. Pieters, B. Racine, E. Quesnel, J. Autschbach, J. Crassous and L. Favereau, *Chem. Sci.*, 2021, **12**, 5522-5533.

15 Z. Yang, Z. Mao, Z. Xie, Y. Zhang, S. Liu, J. Zhao, J. Xu, Z. Chi and M. P. Aldred, *Chem. Soc. Rev.*, 2017, **46**, 915-1016.

16 a) J. P. Riehl and F. S. Richardson, *Chem. Rev.*, 1986, **86**, 1-16; b) E. M. Sánchez-Carnerero, A. R. Agarrabeitia, F. Moreno, B. L. Maroto, G. Muller, M. J. Ortiz and S. de la Moya, *Chem. Eur. J.*, 2015, **21**, 13488-13500; c) H. Tanaka, Y. Inoue and T. Mori, *ChemPhotoChem*, 2018, **2**, 386-402.

17 Peter N. M. Botman, M. Postma, J. Fraanje, K. Goubitz, H. Schenk, Jan H. v. Maarseveen and H. Hiemstra, *Eur. J. Org. Chem.*, 2002, **2002**, 1952-1955.

18 G. W. T. M. J. Frisch, H. B. Schlegel, G. E. Scuseria, , J. R. C. M. A. Robb, G. Scalmani, V. Barone, , H. N. G. A. Petersson, X. Li, M. Caricato, A. V. Marenich, , B. G. J. J. Bloino, R. Gomperts, B. Mennucci, H. P. Hratchian, , A. F. I. J. V. Ortiz, J. L. Sonnenberg, D. Williams-Young, , F. L. F. Ding, F. Egidi, J. Goings, B. Peng, A. Petrone, , D. R. T. Henderson, V. G. Zakrzewski, J. Gao, N. Rega, , W. L. G. Zheng, M. Hada, M. Ehara, K. Toyota, R. Fukuda, , M. I. J. Hasegawa, T. Nakajima, Y. Honda, O. Kitao, H. Nakai, , K. T. T. Vreven, J. A. Montgomery, Jr., J. E. Peralta, , M. J. B. F. Ogliaro, J. J. Heyd, E. N. Brothers, K. N. Kudin, , T. A. K. V. N. Staroverov, R. Kobayashi, J. Normand, , A. P. R. K. Raghavachari, J. C. Burant, S. S. Iyengar, , M. C. J. Tomasi, J. M. Millam, M. Klene, C. Adamo, R. Cammi, , R. L. M. J. W. Ochterski, K. Morokuma, O. Farkas, and D. J. F. J. B. Foresman, *Journal*, 2016. URL: www.gaussian.com.

19 C. Adamo and V. Barone, *J. Chem. Phys.*, 1999, **110**, 6158-6170.

20 a) F. Weigend and R. Ahlrichs, *Phys. Chem. Chem. Phys.*, 2005, **7**, 3297-3305; b) F. Weigend, *Phys. Chem. Chem. Phys.*, 2006, **8**, 1057-1065.

21 G. Scalmani and M. J. Frisch, *J. Chem. Phys.*, 2010, **132**, 114110.

22 S. Grimme, J. Antony, S. Ehrlich and H. Krieg, *J. Chem. Phys.*, 2010, **132**, 154104.

23 a) J. Autschbach, L. Nitsch-Velasquez and M. Rudolph, *Top. Curr. Chem.*, 2011, **298**, 1-98; b) M. Srebro-Hooper and J. Autschbach, *Annu. Rev. Phys. Chem.*, 2017, **68**, 399-420.

24 K. Dhbaibi, L. Favereau, M. Srebro-Hooper, C. Quinton, N. Vanthuyne, L. Arrico, T. Roisnel, B. Jamoussi, C. Poriel, C. Cabanetos, J. Autschbach and J. Crassous, *Chem. Sci.*, 2020, **11**, 567-576.

25 Y. Gao, C. Ren, X. Lin and T. He, *Front. Chem.*, 2020, **8**, 458-458.

26 J. Jiménez, F. Moreno, B. L. Maroto, T. A. Cabreros, A. S. Huy, G. Muller, J. Bañuelos and S. de la Moya, *Chem. Commun.*, 2019, **55**, 1631-1634.

27 R. Bouvier, R. Durand, L. Favereau, M. Srebro-Hooper, V. Dorcet, T. Roisnel, N. Vanthuyne, Y. Vesga, J. Donnelly, F. Hernandez, J. Autschbach, Y. Trolez and J. Crassous, *Chem. Eur. J.*, 2018, **24**, 14484-14494.

28 a) N. Berova, L. D. Bari and G. Pescitelli, *Chem. Soc. Rev.*, 2007, **36**, 914-931; b) N. Harada, K. Nakanishi and N. Berova, in *Comprehensive Chiroptical Spectroscopy*, John Wiley & Sons, Inc., 2012, pp. 115-166.

29 a) L. Di Bari, G. Pescitelli and P. Salvadori, *J. Am. Chem. Soc.*, 1999, **121**, 7998-8004; b) A. Bensalah-Ledoux, D. Pitrat, T. Reynaldo, M. Srebro-Hooper, B. Moore, J. Autschbach, J. Crassous, S. Guy and L. Guy, *Chem. Eur. J.*, 2016, **22**, 3333-3346.

30 *Center for Computational Research, University at Buffalo, http://hdl.handle.net/10477/79221.*